Explicit time-propagation method to treat the dynamics of driven complex systems

Javier Madroñero
Laboratoire de Physique Atomique, Moléculaire et Optique (PAMO), Université catholique de Louvain, 2 chemin du Cyclotron, 1348 Louvain-la-Neuve, Belgium
and Physik Department, Technische Universität München, James-Franck-Straße, 85747 Garching, Germany

Bernard Piraux
Laboratoire de Physique Atomique, Moléculaire et Optique (PAMO), Université catholique de Louvain, 2 chemin du Cyclotron, 1348 Louvain-la-Neuve, Belgium

(Received 15 June 2009; revised manuscript received 27 July 2009; published 9 September 2009)

We describe the efficient implementation of an *explicit* method to solve systems of stiff differential equations either on a grid or within a spectral approach. This method is based on an ansatz that approximates the solution. This ansatz depends on stiffness parameters that are shown to be related to the eigenfrequencies of the system. The accuracy and the performance of the method are tested in three different cases. First, we treat a highly stiff single differential equation, where explicit schemes converge rather slowly. Then, we solve the stationary Schrödinger equation associated to the quantum reflection of an ultracold atom by a surface. Finally, we consider the interaction of atomic hydrogen with a strong low-frequency laser pulse whose duration is of the order of 25 fs. We focus on the calculation of the above-threshold ionization electron spectrum, a problem which, under such realistic physical conditions, is computationally very demanding.

DOI: 10.1103/PhysRevA.80.033409 PACS number(s): 33.20.Xx, 02.60.Cb, 31.15.X−

I. INTRODUCTION

The study of the quantum dynamics of driven complex atomic systems is a fundamental problem in atomic physics and a challenge for both experiments and theory. One illustrative example among others of such a challenge is the two-photon double ionization of He [1–9]. The nonlinearity of this process poses tremendous experimental difficulties that so far prevent the measurement of accurate total and differential cross sections [6,7]. From the theoretical point of view, the full asymptotic behavior of the wave function describing two ejected electrons escaping in the field of the nucleus is not known. It is therefore not surprising that the most elaborate calculations lead to total cross sections that differ by at least one order of magnitude.

One way of studying the dynamics of complex systems is to solve the time-dependent Schrödinger equation (TDSE). Due to the infinite range of the Coulombic interactions, this requires either very large grids or big bases. In both cases, one has to solve large systems of coupled first-order differential equations that are well known to be stiff [10]. By this, it is meant that the time step decreases rapidly with the increasing size of the system. The origin of the stiffness is clear: by increasing the size of the grid or the basis, the diagonalization of the atomic Hamiltonian generates large positive-energy eigenvalues. It is precisely the highest eigenvalue that controls the time step while leading to highly oscillating solutions. In order to overcome this problem, one can use implicit time-propagation methods. This requires to solve very large systems of algebraic equations at each time step. A typical example of such an implicit scheme is the Crank-Nicholson algorithm, which is used in grid methods based on finite differences [11]. This propagation method is tractable when the system is banded but as soon as the complexity of the atomic system increases, the bandwidth of the system increases rapidly together with the computation time. An alternative way of overcoming the stiffness of the problem is to propagate in the atomic basis, where the atomic Hamiltonian is diagonal. Time propagating in the atomic basis has three advantages: first, it is possible to eliminate from the propagation, very high-energy eigenstates that play a minor role in the dynamics. Second, it allows one to work in the interaction picture, where the free evolution of the atomic system is somehow subtracted, and, finally, explicit methods which involve only matrix-vector products are numerically stable in this case. However, this method requires the diagonalization of large matrices, which is a computationally very demanding problem.

In this contribution, we present an alternative explicit method of fourth order for the stiff TDSE. In this method that takes into account the intrinsic frequencies of the system, the solution is expressed in terms of oscillating functions. This leads to a simple recursive formula for the time propagation with a controlled error. At each integration step, only matrix-vector products are therefore needed. In addition, since the method includes the natural oscillations of the system, the time step is typically large. This approach has been introduced by Fatunla about 30 years ago [12,13] but has never been implemented, to the best of our knowledge, in atomic physics. Here, we show that with some modification, this explicit method can be successfully used to solve the TDSE.

The contribution is organized as follows. The description of the algorithm for the solution of stiff differential equations is presented in Sec. II. Two rather simple applications of this method are shown in Sec. III. The first of these is a pure mathematical illustration of a stiff differential equation, where the conventional explicit algorithms converge much more slowly than Fatunla's algorithm. Through the second one, we highlight the physical interpretation of the stiffness parameters of the method in the context of the quantum reflection of an ultracold atom with a surface [14,15]. In Sec.

IV, we consider the interaction of atomic hydrogen with a strong low-frequency laser pulse whose duration is of the order of 25 fs. We focus our attention on the calculation of the above-threshold ionization (ATI) electron spectrum. Although, under the present physical conditions, the ionization process is dominated by tunneling, the ATI spectrum exhibits some features of a resonant behavior. Section V concludes this paper.

II. METHOD

In this section, a brief review of the method proposed in [12,13] is given. Let us start with the m-dimensional *stiff* first-order differential equation,

$$\boldsymbol{y}' = \boldsymbol{f}(x,\boldsymbol{y}), \quad \boldsymbol{y} = (y_1, y_2, \ldots, y_m), \tag{1}$$

where $\boldsymbol{f}(x,y)$ is in general a complex m-dimensional function.

The stiffness of the equation leads to a solution $\boldsymbol{y}(x)$, which is an oscillating function. In a given interval (x_n, x_{n+1}), $x_{n+1}=x_n+h$, with h a small number, $\boldsymbol{y}(x)$ is approximated by the function

$$\boldsymbol{F}(x) = (I - e^{\Omega_1 x})\boldsymbol{a} - (I - e^{-\Omega_2 x})\boldsymbol{b} + \boldsymbol{c}, \tag{2}$$

where I is the identity matrix, $\Omega_i = \mathrm{diag}(\omega_1^{(i)}, \ldots, \omega_m^{(i)})$, $i=1,2$, and $\boldsymbol{a},\boldsymbol{b},\boldsymbol{c}$ are constant vectors. The complex numbers $\omega_1^{(i)}, \ldots, \omega_m^{(i)}$, $i=1,2$ are called *stiffness parameters*. Assuming that $\boldsymbol{F}(x)$ coincides with $\boldsymbol{y}(x)$ at x_n and x_{n+1}, that $\boldsymbol{F}'(x)$ coincides with $\boldsymbol{f}(x,\boldsymbol{y})$ at x_n and that $\boldsymbol{F}''(x)$ coincides with $\boldsymbol{f}'(x,\boldsymbol{y})$ at x_n, the solution $\boldsymbol{y}_{n+1}=\boldsymbol{y}(x_{n+1})$ at x_{n+1} can be expressed recursively in terms of $\boldsymbol{y}_n=\boldsymbol{y}(x_n)$, $\boldsymbol{f}_n=\boldsymbol{f}(x_n,\boldsymbol{y}_n)$, and $\boldsymbol{f}_n^{(1)} = d\boldsymbol{f}/dx|_{x=x_n}$ according to

$$\boldsymbol{y}_{n+1} = \boldsymbol{y}_n + R\boldsymbol{f}_n + S\boldsymbol{f}_n^{(1)}. \tag{3}$$

R and S are diagonal matrices, which can be written in terms of the stiffness parameters,

$$R = \Omega_2\Phi - \Omega_1\Psi, \quad S = \Phi + \Psi, \tag{4}$$

where Φ and Ψ are diagonal matrices, whose nonzero entries are

$$\Phi_i = \frac{e^{\omega_i^{(1)}h} - 1}{\omega_i^{(1)}(\omega_i^{(1)} + \omega_i^{(2)})}, \tag{5}$$

and

$$\Psi_i = \frac{e^{-\omega_i^{(2)}h} - 1}{\omega_i^{(2)}(\omega_i^{(1)} + \omega_i^{(2)})}. \tag{6}$$

Notice that if a stiffness parameter $\omega_i^{(1)}$ ($\omega_i^{(2)}$) vanishes the associated matrix element reads as

$$\Phi_i = \frac{h}{\omega_i^{(2)}} \quad \left(\Psi_i = -\frac{h}{\omega_i^{(1)}}\right). \tag{7}$$

The recursive relation (3) depends on the so far unknown stiffness matrices Ω_1 and Ω_2. However, these matrices can be written in terms of the function $\boldsymbol{f}(x_n,\boldsymbol{y}_n)$ and its derivatives up to third order at x_n. In order to see this, the Taylor expansion of $\boldsymbol{y}_{n+1}=\boldsymbol{y}(x_n+h)$, and the Maclaurin series of $\exp(\Omega_1 h)$ and $\exp(-\Omega_2 h)$,

$$\boldsymbol{y}_{n+1} = \sum_{j=0}^{\infty} \frac{h^j}{j!}\boldsymbol{y}^{(j)}(x_n),$$

$$e^{\Omega_1 h} = \sum_{j=0}^{\infty} \frac{h^j}{j!}\Omega_1^j,$$

$$e^{-\Omega_2 h} = \sum_{j=0}^{\infty} \frac{h^j}{j!}(-1)^j\Omega_2^j, \tag{8}$$

are substituted in the recursion relation (3). The coefficients of h^0, h^1, and h^2 vanish identically. Equating the coefficients of h^3 and h^4 on both sides of Eq. (3) leads to a simple system of algebraic equations for Ω_1 and Ω_2. The components of the stiffness matrices obtained after solving these equations read as [13]

$$\omega_i^{(1)} = \frac{1}{2}[-D_i + \sqrt{D_i^2 + 4E_i}],$$

$$\omega_i^{(2)} = \omega_i^{(1)} + D_i, \tag{9}$$

where D_i and E_i, $i=1,\ldots,m$ are given in terms of the respective components $f_{in}^{(k)}$ of the derivatives $\boldsymbol{f}_n^{(k)}$, $k=0,1,2,3$, of $\boldsymbol{f}(x,\boldsymbol{y})$ at $x=x_n$ by

$$D_i = \frac{f_{in}^{(0)}f_{in}^{(3)} - f_{in}^{(1)}f_{in}^{(2)}}{f_{in}^{(1)}f_{in}^{(1)} - f_{in}^{(0)}f_{in}^{(2)}}, \quad i = 1, \ldots, m, \tag{10}$$

$$E_i = \frac{f_{in}^{(1)}f_{in}^{(3)} - f_{in}^{(2)}f_{in}^{(2)}}{f_{in}^{(1)}f_{in}^{(1)} - f_{in}^{(0)}f_{in}^{(2)}}, \quad i = 1, \ldots, m, \tag{11}$$

provided that the denominator of the previous expressions is nonzero.

The local truncation error at $x=x_{n+1}$ is the difference between the exact solution at x_{n+1} and the numerical solution obtained with the help of Eq. (3). With the assumption that there is no previous error [i.e., $\boldsymbol{y}(x_n)=\boldsymbol{y}_n$], the local truncation error at x_{n+1} can be written as

$$T_{n+1} = \boldsymbol{y}(x_n + h) - \boldsymbol{y}(x_n) - R\boldsymbol{f}(x_n,\boldsymbol{y}_n) - S\boldsymbol{f}^{(1)}(x_n,\boldsymbol{y}_n). \tag{12}$$

By substituting the Taylor expansions of the h-dependent functions involved in the previous equation, it gives [13]

$$\begin{aligned} T_{n+1} &= \frac{h^5}{5!}\frac{1}{\omega_1+\omega_2}[(\omega_1+\omega_2)f_n^{(4)} + (\omega_2^4 - \omega_1^4)f_n^{(1)} \\ &\quad - (\omega_1^4\omega_2 + \omega_1\omega_2^4)f_n^{(0)}] + O(h^6) \\ &= \frac{h^5}{5!}[f_n^{(4)} + (\omega_2^3 - \omega_2^2\omega_1 + \omega_2\omega_1^2 - \omega_1^3)f_n^{(1)} \\ &\quad - \omega_1\omega_2(\omega_1^2 - \omega_1\omega_2 + \omega_2^2)f_n^{(0)}] + O(h^6). \end{aligned} \tag{13}$$

The implementation of the recursion (3) is now rather simple. It requires the calculation of the function $\boldsymbol{f}_n$ and its derivative $\boldsymbol{f}_n^{(1)}$ at each value of x_n. For the stiffness matrices Ω_1 and Ω_2, and thus also for the matrices R and S, the de-

rivatives $\boldsymbol{f}_n^{(2)}$ and $\boldsymbol{f}_n^{(3)}$ are also needed. Ω_1 and Ω_2 have to be calculated in principle at each integration step since they characterize the local frequencies of the solution $\boldsymbol{y}(x)$. However, in all the examples treated in the original papers of Fatunla [12,13], the stiffness matrices were calculated only once at the beginning of the propagation. We found that this procedure is only accurate for functions that exhibit regular oscillations on some range of x (see Sec. III). In addition, the truncation error (13) can be used to control the size of the integration step, e.g., by imposing a boundary criterion for $|T_n|$. For this also, the derivative $\boldsymbol{f}_n^{(4)}$ must be provided.

A special situation occurs when the ith components of $\boldsymbol{y}$ and of the derivatives $f_n^{(k)}$, $k=0,1,2,3$ for a given i are small (comparable with the machine precision). In this case, the denominator in Eqs. (10) and (11) are also small. However, the solution $\boldsymbol{y}(x)$ of Eq. (1) is well behaved and one can expect that the stiffness parameters and, therefore, the matrices R and S have finite moderated values. In this case, the recursion (3) takes the form

$$\boldsymbol{y}_{n+1} = \boldsymbol{y}_n. \tag{14}$$

III. SIMPLE ILLUSTRATIONS

A. Nearly periodic initial value problem

The power of the method can be illustrated in the rather simple case of the differential equation,

$$y'' + y = \alpha e^{ix}, \quad y(0) = 1, \quad y'(0) = \left(1 - \frac{\alpha}{2}\right)i, \tag{15}$$

which admits the following analytical solution:

$$y_1(x) = u(x) + iv(x), \quad \text{with}$$

$$u(x) = \cos x + \frac{\alpha}{2} x \sin x,$$

$$v(x) = \sin x - \frac{\alpha}{2} x \cos x. \tag{16}$$

This equation is also considered in [13] and solved numerically by means of the method described in Sec. II. However, Eq. (15) is there transformed in a set of four *real* coupled differential equations. In order to test the method for a set of *complex* differential equations, we transform the original one into the set of *complex* coupled equations

$$y_1' = y_2 \quad y_1(0) = 1,$$

$$y_2' = -y_1 + \alpha e^{ix} \quad y_2(0) = \left(1 - \frac{\alpha}{2}\right)i. \tag{17}$$

For small values of α, Eq. (16) represents the perturbed motion on a circular orbit in the complex plane, of the point $y(x)=y_1(x)$, which spirals slowly outward such that its distance from the origin at any value of x is given as

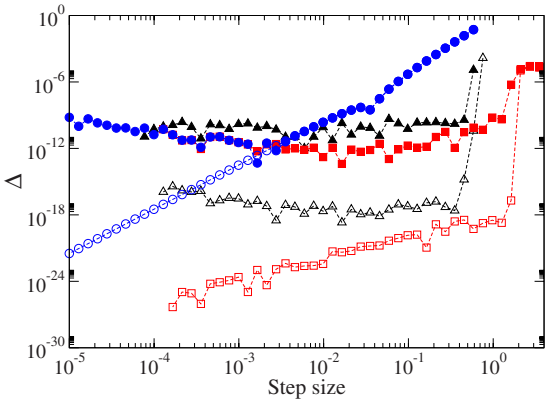

FIG. 1. (Color online) Absolute error $\Delta=|\tau_{\text{exact}}-\tau_{\text{num}}|$ at the end of the integration at $x_{\text{final}}=40\pi$ as function of the fixed step size h of the integrator. Open (filled) symbols are used for calculations using quadruple (single) precision. Results obtained with the help of the recursion formula (3) with the calculation of the stiffness parameters at each integration step are denoted by squares (□,■); absolute error obtained with *only one* calculation of them at the beginning of the integration is shown by triangles (△,▲); error of fourth-order RK method is depicted by circles (○, ●).

$$\tau(x) = |y_1(x)| = \sqrt{1 + \frac{1}{4}\alpha^2 x^2}. \tag{18}$$

Equation (17) is solved numerically for $\alpha=0.001$ in the interval $0 \le x \le 40\pi$ by using the method described in Sec. II and an explicit fourth-order Runge-Kutta (RK) method. In any case, the step size h was kept constant along the integration. For the calculations performed with the recursion (3), the stiffness parameters were calculated either once at the beginning of the integration or successively at each recursion step. Figure 1 shows the absolute error $\Delta=|\tau_{\text{exact}}-\tau_{\text{num}}|$ of the value of $\tau(x)$ obtained at the end of the numerical integration at $x=40\pi$ with respect to the exact value given by Eq. (18). The step size h goes down up to 10^{-5} for the results obtained with RK method (circles). In this case, the accuracy of the calculations scales as h^4. The maximum accuracy is obtained for single precision calculations (filled circles) for a step size around $h=0.001$. The method described in the previous section converges extraordinarily faster: with the help of the recursion (3) with only one calculation of the stiffness matrices and single precision (filled triangles), the accuracy of the results is almost constant for $h<0.4$. It oscillates around $\Delta=5\times10^{-11}$ and reaches a value of $\Delta=3\times10^{-10}$ for $h\approx0.45$. For quadruple precision (open triangles), the situation is similar with the difference that Δ oscillates around 10^{-18}. This reflects the fact that the local frequencies of the solutions $y_1(x)$ and $y_2(x)$ are, in good approximation, constant along the whole real axis, which is a clear consequence of the perturbative character mentioned above for the chosen small value of α. Calculation of the stiffness parameters at each integration step improves significantly the accuracy of the numerical value τ_{num} (squares). Already for a step size of the order of 1, the obtained precision is of the order of 10^{-10} in single precision (filled squares) and of the order of 10^{-18} in quadruple precision (open squares), i.e., the same accuracy

obtained by the RK integrator with a step size, which is three (four) orders of magnitude smaller in single (quadruple) precision.

B. Quantum reflection and the physical interpretation of the stiffness parameters

In this section, we consider the effect of quantum reflection [14–16], which refers to the reflection of particles by attractive long-range potentials in nonclassical regions of coordinate space without reaching a classical turning point. The observation of this effect has been possible due to the advances in cooling techniques during the last years that have enable performing experiments with cold atoms interacting with surfaces [17–21]. The solid surfaces provide a long-range attractive potential for the atoms. For distances shorter than the wavelength of atomic transitions, the interaction is the van der Waals potential of the form $-C_3/r^3$ [22]. At larger distances, the retardation effects become important and the potential takes the form $-C_4/r^4$ [23]. The theoretical description of quantum reflection is then achieved by studying the reflection properties of atoms interacting with the surface through the phenomenological potential [17,24]

$$V(x) = -\frac{C_4}{r^3(r+\lambda)}, \tag{19}$$

which reproduces the van der Waals potential at short distances and the Casimir potential at large distances. The length parameter $\lambda = C_4/C_3$ characterizes the region, where the transition between these two regimes occurs. An atom of mass μ is modeled by an incoming plane wave (at large distance) with energy $E=\hbar^2k^2/2\mu$. Atoms that come too close to the surface are absorbed or undergo inelastic reactions, and, thus, they do not contribute to the effect of quantum reflection. Absorption and inelastic processes are taken into account by incoming WKB boundary conditions in the semiclassical region close to the surface. The corresponding differential equation is thus given by the stationary Schrödinger equation

$$-\frac{\hbar^2}{2\mu}\frac{d^2\Psi}{dr^2} + V(r)\Psi = \frac{\hbar^2k^2}{2\mu}\Psi, \tag{20}$$

with initial conditions

$$\Psi(r_0) = \Psi^{(-)}_{\mathrm{WKB}}(r_0), \qquad \left.\frac{d\Psi}{dr}\right|_{r=r_0} = \left.\frac{d\Psi^{(-)}_{\mathrm{WKB}}}{dr}\right|_{r=r_0}, \tag{21}$$

where r_0 is a small distance to the singularity and $\Psi^{(-)}_{\mathrm{WKB}}(r)$ is the incoming WKB function

$$\Psi^{(-)}_{\mathrm{WKB}}(r) = \frac{T}{\sqrt{p}}\exp\left(-\frac{i}{\hbar}\int p\,dr\right), \tag{22}$$

with transmission coefficient T and momentum $p = \sqrt{2\mu[E+V(r)]}$.

At large distances r_f, the wave function behaves as a superposition of plane waves,

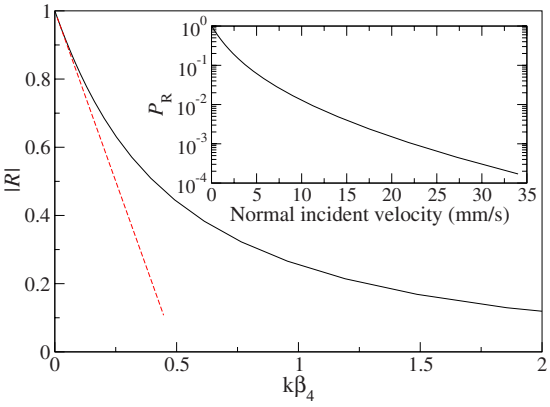

FIG. 2. (Color online) Reflection amplitude $|R|$ for Ne atoms on silicon surfaces as function of the scaled wave number $k\beta_4$ (solid line) compared with the linear threshold behavior $|R|=1-2kb$ (dashed line), with b as the threshold length for the potential (19) given by Eq. (27). In the inset, the reflection probability $|R|^2$ for Ne atoms on silicon surfaces as function of the normal incident velocity is reproduced in perfect agreement with [17].

$$\Psi(r) \sim e^{-ikr_f} + Re^{ikr_f}, \tag{23}$$

and the reflection coefficient R can be expressed in terms of the logarithmic derivative $z=\Psi'(r_f)/\Psi(r_f)$ as

$$R = \frac{ik+z}{ik-z}e^{-2ikr_f}. \tag{24}$$

The reflection amplitude R is obtained after solving numerically the Schrödinger equation (20). For this purpose, Eq. (20) is expressed as a two-dimensional system of differential equations

$$y_1'(x) = -[\tilde{p}(x)]^2 y_2(x), \quad y_2'(x) = y_1(x), \tag{25}$$

where $x=r/\beta_4$ is a dimensionless variable given in terms of the characteristic length of the Casimir potential $\beta_4=\sqrt{2\mu C_4/\hbar^2}$, $\tilde{p}(x)=\sqrt{(k\beta_4)^2-1/[x^3(x+\lambda/\beta_4)]}$ is the scaled classical momentum, and $y_2(x)=\Psi(x\beta_4)$.

By choosing a suitable value of T in Eq. (22), the initial conditions can be written as

$$y_2(x_0) = 1,$$

$$y_1(x_0) = -\left[i\tilde{p}(x_0) + \frac{\tilde{p}'(x_0)}{2\tilde{p}(x_0)}\right]. \tag{26}$$

The initial value problem defined by Eqs. (25) and (26) is then solved with the help of the method described in Sec. II. Figure 2 shows the absolute value of the reflection amplitude as function of the dimensionless wave number $k\beta_4$ for Ne atoms scattering from a silicon surface as in the experiment by Shimizu [17]. In this case, the parameters of the interaction potential (19) are $C_4=6.8\times10^{-56}$ Jm^4 and $\lambda=63.66$ nm $(C_3=C_4/\lambda=1.068\times10^{-48}$ Jm$^3)$. The near-threshold behavior of the reflection amplitude $|R|$ for a particle approaching a long-range attractive potential up to and including linear terms in the asymptotic wave number k is given by $|R| \overset{k\to0}{\sim} 1-2bk+O(k^2)$ [14,15,25]. It is characterized

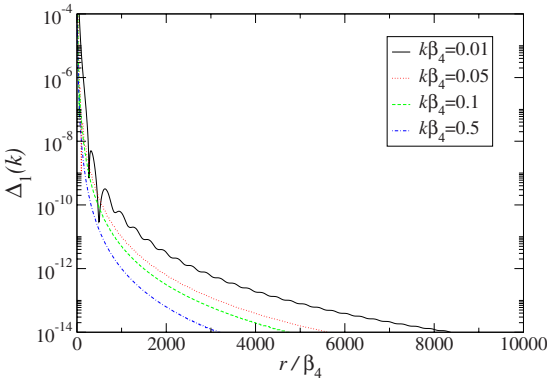

FIG. 3. (Color online) $\Delta_1=\mathrm{Im}(\omega_1)-k$ as function of the distance r/β_4 for $k\beta_4=0.01$, 0.05, 0.1, and 0.5. At short distances, ω_1 varies rapidly due to the presence of the singularity in the potential (19). Asymptotically, Δ_1 vanishes and ω_1 approaches to ik.

by the threshold parameter b, which depends only on the properties of the potential tail beyond a semiclassical region of comparatively "small" distances. For the potential (19), the threshold length is given by [15]

$$b=\frac{\beta_4}{\pi\rho}\frac{1}{J_1^2(2\rho)+Y_1^2(2\rho)}, \tag{27}$$

with $\rho=\sqrt{2\mu}C_3/(\hbar\sqrt{C_4})$, and J_1 and Y_1 are the regular and irregular Bessel functions, respectively. The dashed line in Fig. 2 depicts the linear behavior of $|R|$ near the threshold energy. In addition, the reflection probability $P_R=|R|^2$ shown in the inset in Fig. 2 is in perfect agreement with the theoretical predictions and experimental observations by Shimizu [17].

The complexity of the system (25) is comparable with the complexity of the example treated in Sec. III A. The results presented in Fig. 2 show the accuracy of this approach. In addition to this, we have also investigated the behavior of the stiffness parameters associated to Eq. (25). At short distances, the frequency of the wave function changes rapidly in accordance with the depth of the potential. At large distances, as the wave function approaches its asymptotic form, the stiffness parameters ω_1 and ω_2 tend to the natural frequencies of the system, i.e., $\omega_1\sim ik$ and $\omega_2\sim -ik$, as expected from the ansatz function (2). The difference $\Delta_1=\mathrm{Im}(\omega_1)-k$ as function of the (scaled) distance r/β_4 is shown in Fig. 3 for several values of k. It vanishes at large distances, while $\mathrm{Re}(\omega_1)$ approaches to zero (not shown). A similar behavior is exhibited by ω_2.

IV. RESONANCE STRUCTURES IN THE TUNNELING REGIME OF ATI OF HYDROGEN ATOMS

In this section, we consider hydrogen atoms exposed to intense low-frequency femtosecond laser pulses. We consider linearly polarized light and apply the dipole approximation. In the velocity gauge, the interaction operator reads as

$$V(t)=\boldsymbol{A}(t)\cdot\boldsymbol{p}, \tag{28}$$

where the vector potential takes the form $\boldsymbol{A}(t)=A_0(t)\sin(\omega t)\boldsymbol{e}_z$, for $-\tau/2\le t\le\tau/2$, and zero outside this time interval. $A_0(t)=A_0\cos^2(\pi t/\tau)$ is the envelope containing n_c optical cycles, ω is the pulse angular frequency, $\tau=2\pi n_c/\omega$ is the pulse duration, and $\boldsymbol{e}_z$ is the unit vector along the z axis in the laboratory frame. The Hamiltonian of the driven atom is thus

$$H(t)=H_0+V(t), \tag{29}$$

with

$$H_0=\frac{p^2}{2}-\frac{Z}{r}. \tag{30}$$

We use a spectral representation of the Hamiltonian in terms of spherical harmonics and Coulomb Sturmian functions defined by

$$S_{n\ell}^{(\alpha)}(r)=\sqrt{\frac{(n-\ell-1)!}{2(n+\ell)!}}\left(\frac{2r}{\alpha}\right)^{\ell+1}L_{n-\ell-1}^{2\ell+1}\left(\frac{2r}{\alpha}\right)e^{-r/\alpha}, \tag{31}$$

where $L_n^{(\beta)}(x)$ are the Laguerre polynomials and α is a real number called the dilation parameter.

Substitution of the expansion

$$\psi(\boldsymbol{r},t)=\sum_{n\ell}c_{n\ell}(t)\frac{S_{n\ell}^{(\alpha)}(r)}{r}Y_{\ell m}(\theta,\varphi) \tag{32}$$

of the wave packet $\psi(\boldsymbol{r},t)$ in the TDSE leads to the following matrix representation:

$$iS\frac{d\boldsymbol{y}}{dt}=\mathcal{A}\boldsymbol{y}+g(t)\mathcal{V}\boldsymbol{y}. \tag{33}$$

Here, (i) the overlap matrix S is a block tridiagonal matrix due to the nonorthogonality of the Sturmian basis. Indeed, the nonzero matrix elements satisfy the selection rules $\Delta\ell=0$ and $\Delta n=0,\pm1$.

(ii) $\mathcal{A}$ is the matrix representation of the unperturbed Hamiltonian of the system. It is again a block tridiagonal matrix with selection rules $\Delta\ell=0$ and $\Delta n=0,\pm1$.

(iii) $g(t)=A_0\cos^2(\pi t/\tau)\sin(\omega t)$ is the scalar time-dependent part of the field interaction (28) and $\mathcal{V}$ is the matrix representation of the dipole operator p_z. The selection rules for this matrix are $\Delta\ell=\pm1$ and $\Delta=0,\pm1,\pm2$.

(iv) $\boldsymbol{y}$ is the vector of the coefficients $c_{n\ell}(t)$.

In order to solve numerically the TDSE, the basis (31) has to be truncated: $n_{\max}$ is the number of Sturmian functions per angular configuration for each of the values of $\ell=0,\ldots,\ell_{\max}$. We use the method described in Sec. II for the propagation of the TDSE (33) starting from some initial state represented by the vector $\boldsymbol{y}_0$. According to Eqs. (10), (11), and (13), the derivatives up to fourth order of the function $\boldsymbol{f}(t,\boldsymbol{y})=-iS^{-1}[A\boldsymbol{y}+g(t)V\boldsymbol{y}]$ need to be calculated at each step t_n, where the stiffness parameters and the truncation error are required. These derivatives satisfy the relations

$$iS\boldsymbol{f}_n^{(0)}=[\mathcal{A}+g(t_n)\mathcal{V}]\boldsymbol{y}_n, \tag{34}$$

$$iS\boldsymbol{f}_n^{(1)}=[\mathcal{A}+g(t_n)\mathcal{V}]\boldsymbol{f}_n^{(0)}+g'(t_n)\mathcal{V}\boldsymbol{y}_n, \tag{35}$$

$$iS\boldsymbol{f}_n^{(2)}=[\mathcal{A}+g(t_n)\mathcal{V}]\boldsymbol{f}_n^{(1)}+2g'(t_n)\mathcal{V}\boldsymbol{f}_n^{(0)}+g''(t_n)\mathcal{V}\boldsymbol{y}_n, \tag{36}$$

$$iS\boldsymbol{f}_n^{(3)} = [\mathcal{A} + g(t_n)\mathcal{V}]\boldsymbol{f}_n^{(2)} + 3g'(t_n)\mathcal{V}\boldsymbol{f}_n^{(1)} + 3g''(t_n)\mathcal{V}\boldsymbol{f}_n^{(0)} + g^{(3)}(t_n)\mathcal{V}\mathbf{y}_n, \tag{37}$$

$$iS\boldsymbol{f}_n^{(4)} = [\mathcal{A} + g(t_n)\mathcal{V}]\boldsymbol{f}_n^{(3)} + 4g'(t_n)\mathcal{V}\boldsymbol{f}_n^{(2)} + 6g''(t_n)\mathcal{V}\boldsymbol{f}_n^{(1)} + 4g^{(3)}(t_n)\mathcal{V}\boldsymbol{f}_n^{(0)} + g^{(4)}(t_n)\mathcal{V}\mathbf{y}_n. \tag{38}$$

The vector on the right-hand side of Eq. (34) can be calculated at the beginning of each step. Therefore, $\boldsymbol{f}_n^{(0)}$ can be obtained after solving the system of equations defined by Eq. (34), e.g., using backward substitution. With $\boldsymbol{f}_n^{(0)}$ also the vector on the right-hand side of Eq. (35) is known and, therefore, after backward substitution, $\boldsymbol{f}_n^{(1)}$ can be calculated. Similar procedure holds for $\boldsymbol{f}_n^{(2)}$, $\boldsymbol{f}_n^{(3)}$, and $\boldsymbol{f}_n^{(4)}$.

As a first illustration, we consider the ionization process of the ground state of hydrogen exposed to a laser pulse with frequency $\omega=0.3$ a.u., peak intensity $I=10^{15}$ W/cm^2, and pulse duration 2 fs (83.78 a.u.). With the choice of these parameters, the Keldysh parameter γ is 1.8. The Keldysh parameter [26] is given by

$$\gamma = \sqrt{\frac{I_p}{2U_p}}, \tag{39}$$

where I_p is the ionization potential ($I_p=0.5$ a.u. for atomic hydrogen) and U_p is the ponderomotive energy,

$$U_p = \frac{I}{4\omega^2}, \tag{40}$$

with ω and I as the frequency and intensity of the fields in a.u., respectively. When $\gamma \gg 1$, the system is considered to be in the multiphoton regime and when $\gamma \ll 1$, in the tunneling regime. Therefore, for the parameters chosen above the process lies in the multiphoton regime. In this case, the ionized electron absorbs a number of additional photons from the field while still influenced by the Coulomb potential [27]. The energy spectrum exhibits peaks which positions are given by

$$E_n = n\omega - U_p - I_p. \tag{41}$$

The first two peaks can be observed in the calculated energy spectrum depicted in Fig. 4. From the numerical point of view, this is not a demanding problem: this is a two-photon ionization process. A diagonally implicit RK scheme [28–30] solves rather efficiently the TDSE in this case and has been used as a reference for comparison with our alternative method. In Fig. 4 we compare the electron energy spectrum as well as the population of the ground state during the interaction with the pulse (inset) obtained with Fatunla propagator (solid lines) and with a diagonally implicit RK method (dashed lines). Converged results are already obtained with a small basis of $n_{\max}=100$ and $\ell_{\max}=10$ with an optimal value of the dilation parameter α around 2.5 (though we have gone up to $n_{\max}=400$ and $\ell_{\max}=10$). The algorithm described in Sec. II does not implicitly preserve the norm—as all explicit methods, such as RK. Therefore, in addition to the size of the basis and the stability of the results with respect to the parameter α, the accuracy of the norm can be also used as a convergence criterion. For the case we are concerned now,

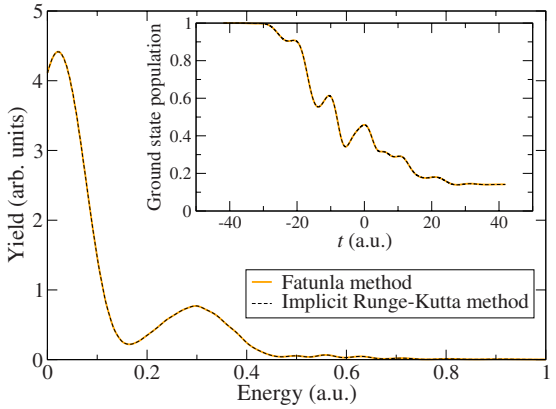

FIG. 4. (Color online) Population of the ground state of hydrogen after ionization by a $I=10^{15}$ W/cm^2 laser pulse with frequency $\omega=0.3$ a.u. and number of cycles $n_c=4$. Time propagation obtained with the method described in Sec. II (solid line) and with a diagonally implicit scheme of a RK propagator (dashed line). Both results coincide within three digits at the end of the pulse. The same situation is observed for the energy spectrum displayed in the inset.

the norm at the end of the integration is 0.999 995. This can be improved by reducing the value of the allowed truncation error (13) ($|T_n| \leq 10^{-10}$ in our case), which controls the step size. The degree of stiffness of the TDSE is reflected in this case in the fact that the stiffness parameters (9) are needed to be calculated at each integration step (otherwise, the norm of the wave function becomes much larger than 1). Nevertheless, the computation time compared with the time needed by the diagonally implicit RK integrator is at least ten times smaller (e.g., for $n_{\max}=100$, $\ell_{\max}=10$, and $\alpha=2.5$, RK takes more than 300 s, while our algorithm takes 20 s).

Now we turn to the interaction of atomic hydrogen with intense femtosecond infrared laser pulses. We consider the ionization process from the ground state of atomic hydrogen exposed to a laser pulse of 790 nm ($\omega=0.057$ a.u.), which is chosen to match the Ti:sapphire lasing frequency, and peak intensities 4×10^{14} and 6×10^{14} W/cm^2. The Keldysh parameter for this choice is $\gamma=0.533$ and $\gamma=0.435$, respectively. We consider a pulse of $n_c=10$ optical cycles, which corresponds to a pulse duration of about 25 fs (1102.3 a.u.). The laser parameters are chosen in this way in order to match those of Rudenko *et al.*'s experiment [31].

At intensities of the order of 10^{14}–10^{15} W/cm^2 and infrared frequencies, there is no clear separation between the regime where multiphoton processes dominate the ionization of atoms exposed to such fields and the strong-field limit dominated by tunnel ionization. In fact, there is a subtle interplay between the two mechanisms as indicated by the fact that the Keldysh parameter is still close to one. For instance, Rudenko's experiment on ionization of rare atoms in this regime shows evidence [31] of resonance structures in the electron ATI spectrum, which are thought to be characteristic of the multiphoton regime. Another experiment [32] in the same regime shows however that the ionization rate follows adiabatically the oscillations of the field.

Understanding the interplay of such mechanisms poses a challenge for both experiment and theory. From the theoretical point of view, one of the main difficulties to deal with

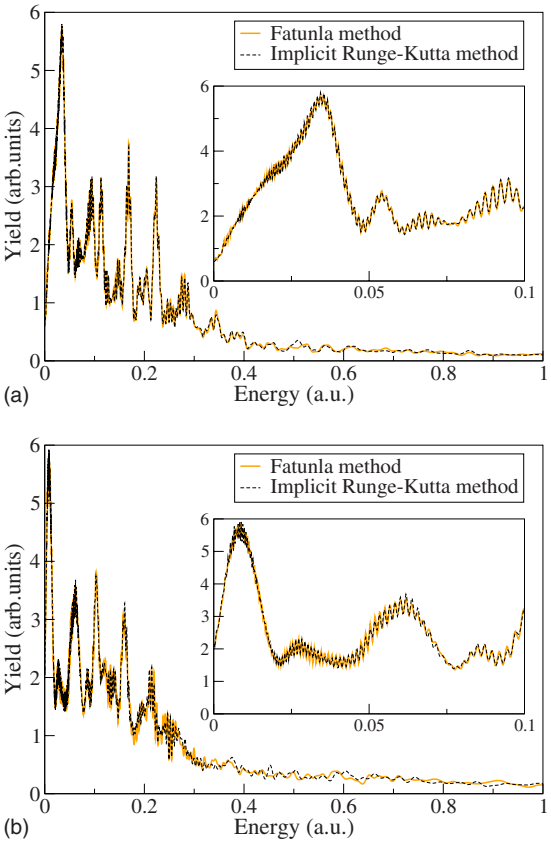

FIG. 5. (Color online) Energy spectrum for hydrogen driven by a field with frequency $\omega=0.057$ a.u. and intensities $I=4\times10^{14}$ W/cm^2 (top) and $I=6\times10^{14}$ W/cm^2 (bottom). Results obtained for several $n_{\mathrm{sup}}=400$, $\ell_{\mathrm{max}}=50$, and $\alpha=2.5$ ($\kappa=1/\alpha=0.4$. The dashed curve was obtained using a diagonally implicit RK propagator. The solid curve was obtained using Fatunla's method.

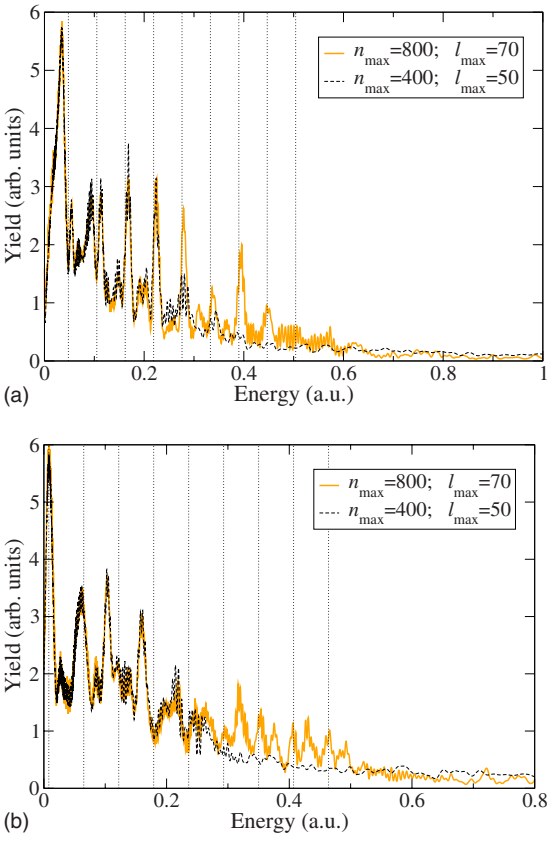

FIG. 6. (Color online) Electron energy distributions for single ionization of hydrogen by 25 fs pulses at $I=4\times10^{14}$ W/cm^2 (top) and $I=6\times10^{14}$ W/cm^2 (bottom). Convergence of the results as a function of the basis size: $n_{\mathrm{max}}=800$ and $\ell_{\mathrm{max}}=70$ (solid line); $n_{\mathrm{max}}=400$ and $\ell_{\mathrm{max}}=50$ (dashed line). The dotted vertical lines denote the expected position of the peaks according to Eq. (41).

this regime is the solution of the TDSE, which requires an accurate treatment of the very high-order angular momentum coupling in this regime of low frequency, rather long pulse duration and high-field intensity. This can be seen in the processes considered here by the number of photons required for the ionization: 24 (31) photons at 4×10^{14} W/cm^2 (at 6×10^{14} W/cm^2). Some features of the energy spectrum at low energy can be already seen by coupling at least 40 angular momenta with $n_{\mathrm{max}}=400$. Figure 5 shows the energy spectra at 4×10^{14} W/cm^2 (top) and at 6×10^{14} W/cm^2 (bottom) obtained with $n_{\mathrm{max}}=400$ and $\ell_{\mathrm{max}}=50$. The results obtained with our approach are compared with those obtained with a diagonally implicit RK method. The accuracy of both approaches is evident, however, the main difference is the efficiency: while our approach needs around 12 h for a single run, under the same conditions the diagonally implicit RK algorithm requires ten times longer. These results are stable against small variation of α and the norm at the end of the integration using Fatunla integrator is 1.0001 ± 0.0002 in this case. Figure 6 displays the energy spectrum for the same intensities as above obtained with 800 Sturmian functions for each angular momentum $\ell=0,\ldots,70$ (a single run requires more than one week; a factor of 10 is expected for RK). These yields are compared with the yields obtained with $n_{\mathrm{max}}=400$. The low-energy part of the spectrum is reproduced by the small basis. It consists of peaks which are rather irregularly distributed, specially in the case of $I=6\times10^{14}$ W/cm^2. A region for higher energies can be only resolved with the larger basis. The dotted vertical lines in Fig. 6 indicate the positions of the peaks as expected from Eq. (41). For $I=4\times10^{14}$ W/cm^2, only some peaks in the high-energy regime of the spectrum coincide with the expectations from the multiphoton regime. The low-energy spectrum, by contrast, is dominated by peaks irregularly distributed. This irregular behavior of the peaks is highlighted in the ATI spectrum at $I=6\times10^{14}$ W/cm^2.

Understanding the origin of these structures is not the purpose of the present contribution. It requires further investigation and will be presented elsewhere.

V. CONCLUSIONS

We presented an efficient implementation of an explicit algorithm for the solution of stiff differential equations. It is therefore suitable for the propagation of the TDSE in a spectral or grid representation. The algorithm is based on the ansatz (2), which approximates the solution of the differential equation in terms of oscillating functions. Appropriate matching conditions at each integration step leads to a simple

recursive formula, which implementation requires only matrix-vector products.

The accuracy and performance of this method were tested in several cases. A simple mathematical stiff differential equation, where other explicit methods converge slowly compared with Fatunla's algorithm; in the process of reflection of ultracold atoms by surfaces, which allowed us to highlight the intrinsic nature of the stiffness parameters and, finally, in the ionization process of hydrogen atoms by intense fields. Special attention was given to the case of femtosecond infrared intense laser pulses. In this regime, where the Keldysh parameter is close to 1, some structures in the ATI energy spectrum were found, which can be only partially associated to multiphoton ionization peaks. The nature of the remaining structures still remains unclear and deserves further investigation.

Our calculations show a stupendous efficiency compared to diagonally implicit propagation algorithms. This opens perspectives for the treatment of complicate ionization processes such as two-photon ionization of helium. From the practical point of view, the implementation of our approach using a spectral representation, e.g., the one described in [33–35], is straightforward. It requires only matrix-vector products. On the other hand, Fatunla's method allows us to time propagate directly in the Sturmian basis without having to solve huge systems of algebraic equations at each time step and without the necessity of fully diagonalizing the atomic Hamiltonian.

ACKNOWLEDGMENTS

The authors are indebted to Robin Shakeshaft for bringing [12] to their attention. J.M. thanks the support by the FNRS ("Bourse postdoctorale FNRS dans le cadre de la convention IISN No. 4.4.503.02"). This contribution is part of an ongoing research supported by the COST action CM0702 of the European Community.

[1] L. Feng and H. W. van der Hart, J. Phys. B **36**, L1 (2003).
[2] R. Shakeshaft, Phys. Rev. A **76**, 063405 (2007).
[3] L. A. A. Nikolopoulos and P. Lambropoulos, J. Phys. B **40**, 1347 (2007).
[4] E. Foumouo, P. Antoine, B. Piraux, L. Malegat, H. Bachau, and R. Shakeshaft, J. Phys. B **41**, 051001 (2008).
[5] A. S. Kheifets and I. A. Ivanov, J. Phys. B **39**, 1731 (2006).
[6] A. Rudenko *et al.*, Phys. Rev. Lett. **101**, 073003 (2008).
[7] P. Antoine, E. Foumouo, B. Piraux, T. Shimizu, H. Hasegawa, Y. Nabekawa, and K. Midorikawa, Phys. Rev. A **78**, 023415 (2008).
[8] D. A. Horner, F. Morales, T. N. Rescigno, F. Martín, and C. W. McCurdy, Phys. Rev. A **76**, 030701(R) (2007).
[9] A. Palacios, T. N. Rescigno, and C. W. McCurdy, Phys. Rev. A **79**, 033402 (2009).
[10] E. Hairer and G. Wanner, *Solving Ordinary Differential Equations II: Stiff and Differential-Algebraic Problems* (Springer-Verlag, Berlin, 1991).
[11] C. Cerjan and K. C. Kulander, Comput. Phys. Commun. **63**, 529 (1991).
[12] S. O. Fatunla, Math. Comput. **32**, 1 (1978).
[13] S. O. Fatunla, Math. Comput. **34**, 373 (1980).
[14] R. Côté, H. Friedrich, and J. Trost, Phys. Rev. A **56**, 1781 (1997).
[15] H. Friedrich, G. Jacoby, and C. G. Meister, Phys. Rev. A **65**, 032902 (2002).
[16] F. Arnecke, H. Friedrich, and J. Madroñero, Phys. Rev. A **74**, 062702 (2006).
[17] F. Shimizu, Phys. Rev. Lett. **86**, 987 (2001).
[18] T. A. Pasquini, Y. Shin, C. Sanner, M. Saba, A. Schirotzek, D. E. Pritchard, and W. Ketterle, Phys. Rev. Lett. **93**, 223201 (2004).
[19] T. A. Pasquini, M. Saba, G.-B. Jo, Y. Shin, W. Ketterle, D. E. Pritchard, T. A. Savas, and N. Mulders, Phys. Rev. Lett. **97**, 093201 (2006).
[20] H. Oberst, D. Kouznetsov, K. Shimizu, J. I. Fujita, and F. Shimizu, Phys. Rev. Lett. **94**, 013203 (2005).
[21] D. Kouznetsov and H. Oberst, Phys. Rev. A **72**, 013617 (2005).
[22] G. Vidali, G. Ihm, H.-Y. Kim, and M. W. Cole, Surf. Sci. Rep. **12**, 135 (1991).
[23] H. B. G. Casimir and D. Polder, Phys. Rev. **73**, 360 (1948).
[24] V. Druzhinina and M. DeKieviet, Phys. Rev. Lett. **91**, 193202 (2003).
[25] H. Friedrich and J. Trost, Phys. Rep. **397**, 359 (2004).
[26] L. V. Keldysh, Sov. Phys. JETP **20**, 1307 (1965).
[27] P. Agostini, F. Fabre, G. Mainfray, G. Petite, and N. K. Rahman, Phys. Rev. Lett. **42**, 1127 (1979).
[28] E. Huens, B. Piraux, A. Bugacov, and M. Gajda, Phys. Rev. A **55**, 2132 (1997).
[29] P. J. Van Der Houwen, B. P. Sommeijer, and W. Couzy, Math. Comput. **58**, 135 (1992).
[30] R. Alexander, SIAM (Soc. Ind. Appl. Math.) J. Numer. Anal. **14**, 1006 (1977).
[31] A. Rudenko, K. Zrost, C. D. Schröter, V. L. B. de Jesus, B. Feuerstein, R. Moshammer, and J. Ullrich, J. Phys. B **37**, L407 (2004).
[32] M. Uiberacker *et al.*, Nature (London) **446**, 627 (2007).
[33] G. Lagmago Kamta, B. Piraux, and A. Scrinzi, Phys. Rev. A **63**, 040502(R) (2001).
[34] J. Eiglsperger, B. Piraux, and J. Madroñero, Phys. Rev. A **80**, 022511 (2009).
[35] E. Foumouo, G. L. Kamta, G. Edah, and B. Piraux, Phys. Rev. A **74**, 063409 (2006).